Hybrid functionals based on a screened Coulomb potential

Jochen Heyd and Gustavo E. Scuseria
Department of Chemistry, Rice University, Houston, Texas 77005-1892

Matthias Ernzerhof
Département de Chimie, Université de Montréal, Montréal, Québec H3C 3J7, Canada

(Received 2 December 2002; accepted 5 February 2003)

Hybrid density functionals are very successful in describing a wide range of molecular properties accurately. In large molecules and solids, however, calculating the exact (Hartree–Fock) exchange is computationally expensive, especially for systems with metallic characteristics. In the present work, we develop a new hybrid density functional based on a screened Coulomb potential for the exchange interaction which circumvents this bottleneck. The results obtained for structural and thermodynamic properties of molecules are comparable in quality to the most widely used hybrid functionals. In addition, we present results of periodic boundary condition calculations for both semiconducting and metallic single wall carbon nanotubes. Using a screened Coulomb potential for Hartree–Fock exchange enables fast and accurate hybrid calculations, even of usually difficult metallic systems. The high accuracy of the new screened Coulomb potential hybrid, combined with its computational advantages, makes it widely applicable to large molecules and periodic systems. © *2003 American Institute of Physics.*
[DOI: 10.1063/1.1564060]

I. INTRODUCTION

In recent years, density functional theory (DFT) has proven to be a highly competitive method in a wide range of applications. While the local density approximation (LDA) has been used in solid state physics for quite some time, the advent of functionals based on the generalized gradient approximation (GGA)[1] has made DFT a valuable tool in chemistry. Hybrid density functionals,[2] which include a certain amount of Hartree–Fock (HF) exchange, have further improved upon the GGA results. This improvement apparently originates in the inclusion of nondynamical correlations which effectively delocalize the GGA exchange hole. Efficient hybrid calculations of solids are possible using Gaussian-type orbitals and periodic boundary conditions (PBC).[3,4] More recently, linear scaling DFT and HF methods[5–7] have become available, drastically reducing the cost of calculations for large systems.

Long-range Coulomb interactions can be calculated efficiently for extended systems using techniques based on the fast multipole method (FMM).[4,8–12] Unfortunately, this approach cannot be used for the HF exchange interaction, since FMM relies on a specific contraction scheme between the electron repulsion integrals and the density matrix.

Kohn has shown that the range of the exchange interaction in insulators decays exponentially as a function of the HOMO–LUMO or band gap.[13] In metallic systems, our own benchmarks indicate that the decay is algebraic. Various truncation schemes have been proposed[6,14,15] to exploit the exponential decay in systems with sizable band gaps. However, these approaches fail to significantly decrease the computational effort in systems with small or no gaps. This greatly increases time demands of hybrid calculations, compared to pure DFT calculations, i.e., those without a portion of HF exchange.

In our PBC calculations, HF exchange is calculated in real space as the sum over all significant interactions in the unit cell and between the unit cell and its neighbors (see Sec. III). An example of a PBC HF calculation on a (6,6) metallic carbon nanotube is shown in Fig. 1. The squares depict the HF exchange energy contribution of a given cell as a function of distance from the reference cell. As mentioned above, convergence with distance is very slow in metallic systems and full convergence of HF calculations is extremely hard to achieve.

In solid state physics, screening of the Coulomb potential has a long history.[16] HF calculations in metals suffer from a divergence in the derivative of the orbital energies with respect to k.[17] This singularity is caused by the divergence of the Fourier transform $4\pi/k^2$ of the $1/r$ Coulomb potential which diverges for $k=0$. A screened potential, having a shorter range than $1/r$, eliminates the divergence. More recently, screened Coulomb potentials have also been used in quantum chemistry[18–21] for different purposes.

In this work, we propose to apply a screened Coulomb potential *only* to the *exchange* interaction in order to screen the long-range part of the HF exchange. All other Coulomb interactions of the Hamiltonian, such as the Coulomb repulsion of the electrons, will *not* use a screened potential. We split the Coulomb operator into short-range (SR) and long-range (LR) components:

$$\frac{1}{r}=\underbrace{\frac{\mathrm{erfc}(\omega r)}{r}}_{\mathrm{SR}}+\underbrace{\frac{\mathrm{erf}(\omega r)}{r}}_{\mathrm{LR}}, \tag{1}$$

where $\mathrm{erfc}(\omega r)=1-\mathrm{erf}(\omega r)$ and ω is an adjustable parameter.

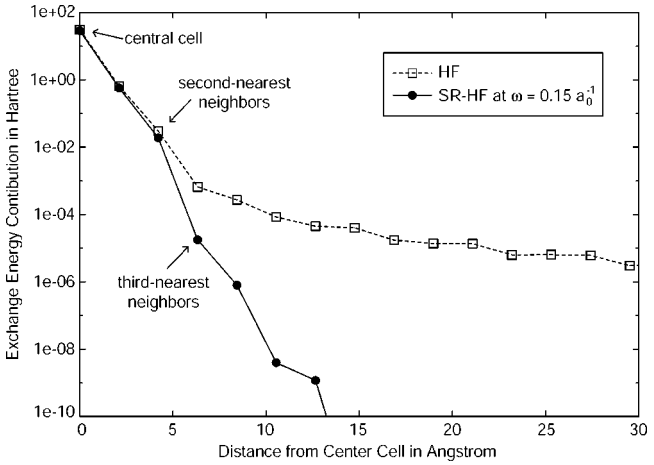

FIG. 1. Comparison of decay properties of unscreened (traditional) and short-range HF exchange in a metallic (6,6) carbon nanotube. Exchange energy contribution of a cell vs its distance from the central (reference) cell.

For $\omega=0$, the long-range term becomes zero and the short-range term is equivalent to the full Coulomb operator. The opposite is true for $\omega\to\infty$. The choice of the error function is somewhat arbitrary but sensible in our case, because the error function can be integrated analytically when using Gaussian basis functions.

Figure 1 shows the effect of using such a screened Coulomb potential for the HF exchange interaction in a metallic system (circles). The screened exchange energy contribution decays exponentially as a function of distance, even though the system has no band gap. In insulators (not shown here), the already present exponential decay is accelerated even further.

II. A SCREENED COULOMB POTENTIAL HYBRID FUNCTIONAL

We propose a new hybrid functional which performs the exact exchange mixing only for short-range interactions in both HF and DFT. This allows the exchange hole to become delocalized among the near neighbors of a reference point, but not beyond.

The PBE0 hybrid functional,[22–25] which is based on the PBE exchange–correlation functional by Perdew *et al.*,[26] assumes the following form for the exchange–correlation energy:

$$E_{xc}^{\mathrm{PBE0}}=aE_x^{\mathrm{HF}}+(1-a)E_x^{\mathrm{PBE}}+E_c^{\mathrm{PBE}}, \tag{2}$$

where the mixing coefficient $a=1/4$ is determined by perturbation theory.[22] We focus now on the expression for the exchange energy

$$E_x^{\mathrm{PBE0}}=aE_x^{\mathrm{HF}}+(1-a)E_x^{\mathrm{PBE}} \tag{3}$$

and split all terms into their short- and long-range components:

$$E_x^{\mathrm{PBE0}}=aE_x^{\mathrm{HF,SR}}(\omega)+aE_x^{\mathrm{HF,LR}}(\omega)+(1-a)E_x^{\mathrm{PBE,SR}}(\omega)+E_x^{\mathrm{PBE,LR}}(\omega)-aE_x^{\mathrm{PBE,LR}}(\omega). \tag{4}$$

Numerical tests based on realistic ω values (e.g., $\omega=0.15$ as in Fig. 1) indicate that the HF and PBE long-range exchange contributions of this functional are rather small (just a few percent), and that these terms tend to cancel each other. Thus, if we neglect them and work under the assumption that this approximation may be compensated by other terms in the functional, we obtain a screened Coulomb potential hybrid density functional of the form:

$$E_{xc}^{\omega\mathrm{PBEh}}=aE_x^{\mathrm{HF,SR}}(\omega)+(1-a)E_x^{\mathrm{PBE,SR}}(\omega)+E_x^{\mathrm{PBE,LR}}(\omega)+E_c^{\mathrm{PBE}}, \tag{5}$$

where ω is an adjustable parameter governing the extent of short-range interactions. The ωPBE hybrid, or ωPBEh, is equivalent to PBE0 for $\omega=0$ and asymptotically reaches PBE for $\omega\to\infty$. A derivation of the various short- and long-range terms in (5) is outlined in the following sections.

A. Screened Coulomb potential Hartree–Fock exchange

The short-range component of the HF exchange can be obtained by using the SR Coulomb potential when calculating the electron repulsion integrals (ERI) for the HF exchange energy.[27,28] The PRISM algorithm[29] can be modified to generate the short-range ERI,

$$(\mu\nu|\lambda\sigma)^{\mathrm{SR}}=\int\int d\mathbf{r}_1\,d\mathbf{r}_2\,\phi_\mu(\mathbf{r}_1)\phi_\nu(\mathbf{r}_1)\times\frac{\mathrm{erfc}(\omega r_{12})}{r_{12}}\phi_\lambda(\mathbf{r}_2)\phi_\sigma(\mathbf{r}_2), \tag{6}$$

over contracted Gaussian-type basis functions $\phi_i(r)$. It is only necessary to modify the fundamental $[0]^{(m)}$ integrals, from which the ERIs are generated by recursion,

$$[0]^{(m),\mathrm{SR}}=U[(2\theta^2)^{m+1/2}G_m(T)-(2\theta_\omega^2)^{m+1/2}G_m(T_\omega)], \tag{7}$$

where

$$G_m(T)=(2/\pi)^{1/2}\int_0^1 dt\,t^{2m}\exp(-Tt^2),$$

$$\theta^2=\left(\frac{1}{\zeta}+\frac{1}{\eta}\right)^{-1},\quad T=\theta^2R^2,$$

$$\theta_\omega^2=\left(\frac{1}{\zeta}+\frac{1}{\eta}+\frac{1}{\omega^2}\right)^{-1},\quad T_\omega=\theta_\omega^2R^2,$$

and U, R, ζ, and η are derived from the basis functions via the Gaussian product rule (see Ref. 29). Evaluating the short-range ERIs is only slightly more time consuming than the regular ERIs since only the primitive $[0]^{(m)}$ integrals are modified. The contraction and transformation steps of the PRISM algorithm dominate the computational time and remain unchanged.

B. A screened Coulomb potential PBE exchange functional

The screened Coulomb exchange functional is based on a short-range modification of the PBE exchange functional.[26] The exchange hole of the PBE functional has been constructed in Ref. 30. Here we use this hole as a starting point and scale it by the SR Coulomb screening factor:

$$J^{\omega\mathrm{PBE,SR}}(\rho,s,y)=J^{\mathrm{PBE}}(s,y)\times\mathrm{erfc}\left(\frac{\omega y}{k_F}\right), \tag{8}$$

where $s=|\nabla\rho|/2k_F\rho$ is the reduced gradient and $k_F=(3\pi^2\rho)^{1/3}$. We then integrate the exchange hole to yield the enhancement factor

$$F_x^{\omega\mathrm{PBE,SR}}(\rho,s)=-\tfrac{8}{9}\int_0^\infty dy\, yJ^{\omega\mathrm{PBE,SR}}(\rho,s,y). \tag{9}$$

This enhancement factor includes not only the PBE gradient correction to LDA, but also the Coulomb screening for the short range. Further details about the derivation of (9) can be found in the Appendix.

Multiplying the enhancement factor with the LDA exchange energy density $\epsilon_x^{\mathrm{LDA}}$ then yields the exchange energy density for the short-range ωPBE functional:

$$\epsilon_x^{\omega\mathrm{PBE,SR}}(\rho(\mathbf{r}),s(\mathbf{r}))=\epsilon_x^{\mathrm{LDA}}(\rho(\mathbf{r}))F_x^{\omega\mathrm{PBE,SR}}(\rho(\mathbf{r}),s(\mathbf{r})). \tag{10}$$

Integrating $\epsilon_x^{\omega\mathrm{PBE,SR}}$ over all space results in the short-range ωPBE exchange energy contribution,

$$E_x^{\omega\mathrm{PBE,SR}}=\int d\mathbf{r}\,\rho(\mathbf{r})\epsilon_x^{\omega\mathrm{PBE,SR}}(\rho(\mathbf{r}),s(\mathbf{r})). \tag{11}$$

The long-range term can be calculated as

$$E_x^{\omega\mathrm{PBE,LR}}=\int d\mathbf{r}\,\rho(\mathbf{r})[\epsilon_x^{\mathrm{PBE}}(\rho(\mathbf{r}),s(\mathbf{r}))-\epsilon_x^{\omega\mathrm{PBE,SR}}(\rho(\mathbf{r}),s(\mathbf{r}))]. \tag{12}$$

Modifying the exchange hole to include the screened Coulomb potential changes the normalization of the hole. The resulting ωPBE–SR (or LR) functional can therefore only be used in calculations where *all* Coulomb interactions use a screened potential or in a hybrid functional (like ωPBEh) which compensates for this.

III. COMPUTATIONAL DETAILS

Due to the complexity of the ωPBE functional, it was deemed simpler, for testing purposes, to use a two-dimensional cubic spline interpolation to calculate the first derivatives with respect to the density ρ and the reduced gradient s. A 1600×1600 grid in $\log(\rho)$ and s is used, yielding 10^{-10} accuracy for the enhancement factor $F_X^{\omega\mathrm{PBE,SR}}(s)$ and 10^{-9} for its derivatives. These derivatives were used for both self-consistent energy calculations as well as geometry optimizations with analytic gradients.

The ωPBEh functional was incorporated into the development version of GAUSSIAN.[31] The 6-311++G($3df$,$3pd$) basis set was used in self-consistent Kohn–Sham calculations of atomic energies, enthalpies of formation, and geometry optimizations of diatomic molecules. This basis is large enough to achieve results close to the basis set limit.

All thermodynamical data was calculated using geometries optimized at the MP2/6-31G* level. Standard enthalpies of formation were obtained by the procedure described in Ref. 32. For both the zero point energy and the thermal enthalpy corrections, HF/6-31G* frequencies scaled with a factor of $f=0.8929$ were used.

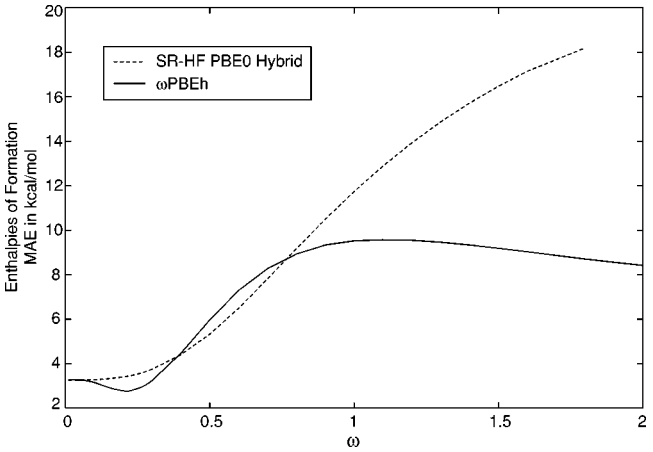

FIG. 2. Mean absolute error in standard enthalpies of formation of the G2-1 set (55 molecules): SR HF PBE0 hybrid compared to ωPBEh as a function of ω.

The PBC calculations of carbon nanotubes were performed with a PBC implementation[4] in GAUSSIAN. A generalized version of the near field exchange (NFX)[6] was used to evaluate the HF exchange in periodic systems. Geometries were optimized at the PBE/6-31G level. The 6-31G* basis set was employed for the density of states calculations.

IV. RESULTS AND DISCUSSION

In order to validate our assumption in Sec. II, we compare the new ωPBEh functional to a PBE0-like hybrid which uses the screened SR HF exchange instead of the full HF exchange,

$$E_{xc}^{\mathrm{SR,HF\ PBE0}}=aE_x^{\mathrm{HF,SR}}+(1-a)E_x^{\mathrm{PBE}}+E_c^{\mathrm{PBE}}, \tag{13}$$

where $a=1/4$. Mean absolute errors (MAE) for standard enthalpies of formation at 298 K were calculated as a function of ω. Results for the G2-1 set of 55 small molecules[32] are shown in Fig. 2. For $\omega=0$, ωPBEh reproduces PBE0 (up to a slight deviation due to the parametrization of the PBE and ωPBE exchange holes). ωPBEh reduces to the nonhybrid PBE functional for $\omega\to\infty$. The computational effort necessary to calculate the SR HF exchange decreases drastically with increasing ω.

An extensive study of the ω dependence of various properties was performed for both molecules and solids. All calculated molecular properties only show a very slight dependence on ω in the range from $\omega=0.05$ to $0.35\ a_0^{-1}$, which validates our earlier assumption. In order to reproduce reliable values for the band gap in semiconducting solids, it is necessary to choose $\omega\leqslant0.15$. In these systems, the calculated band gap is directly proportional to the HF contribution to the exchange energy.

In addition, two-dimensional optimizations of both a and ω were carried out over the G2-1 set of small molecules and for selected periodic systems. The minima in parameter space were very broad and give no reason to change the mixing coefficient $a=1/4$.

A balanced description that provides good accuracy and speed, both in molecules and solids, can be achieved by choosing $\omega=0.15\ a_0^{-1}$. This value will be used hereafter.

TABLE I. Total nonrelativistic energies of atoms (in hartrees).[a]

Atom	Exact[b]	PBE	PBE0	ωPBEh
H	−0.500	−0.500	−0.501	−0.511
He	−2.904	−2.891	−2.894	−2.916
Li	−7.478	−7.460	−7.466	−7.496
Be	−14.667	−14.628	−14.635	−14.676
B	−24.654	−24.609	−24.617	−24.672
C	−37.845	−37.794	−37.803	−37.871
N	−54.589	−54.529	−54.540	−54.621
O	−75.067	−75.005	−75.013	−75.107
F	−99.734	−99.661	−99.667	−99.775
Ne	−128.938	−128.846	−128.851	−128.971

[a]6-311++G($3df$,$3pd$) basis set.
[b]Exact atomic energies from Ref. 37.

Table I shows the total energies for the H–Ne atoms, comparing the new ωPBEh functional to PBE and PBE0. The modest underestimation of the total energies is due to different decay properties of HF and DFT exchange energy potentials. The more delocalized SR–HF exchange falls off slightly slower for $\omega>0$ than the LR–DFT exchange increases. This produces a slight overall increase in the magnitude of the exchange energy, due to an overcompensation by the LR–DFT part. In addition, the lack of self-interaction correction in the PBE correlation functional contributes to the underestimation of the total energies.

A. Standard enthalpies of formation

Tables II and III show the results for standard enthalpies of formation for both the G2-1 and the larger G2-2 set of molecules. The performance of ωPBEh is better than PBE0 for both test sets and only slightly worse than that of B3LYP which contains empirical parameters fitted on the G2-1 set of molecules. The reason for the improvement over PBE0 is twofold: First, the underlying (exchange hole based) form of PBE predicts better thermodynamical properties (in the order of 0.5 kcal/mol for the MAE). Second, the dip in the mean absolute error at $0.1\leqslant\omega\leqslant0.3$ for the G2-1 set (see Fig. 2) also improves the results.

Not surprisingly, the magnitude of errors for individual molecules closely resembles the PBE0 errors. Overall, the performance of ωPBEh for calculating enthalpies of formation is on par with the best established hybrid functionals.

B. Geometry optimizations

Bond length optimizations were carried out for the 22 diatomic molecules of the G2-1 set and compared to experiment.[33] The results are summarized in Table IV. Again, the performance of ωPBEh is as good or better than the results from the established hybrid DFT methods B3LYP and PBE0.

C. Periodic boundary condition calculations

In order to evaluate the performance of ωPBEh in periodic systems, PBC calculations were carried out on several carbon single-walled nanotubes (SWNT). This provides some insights in terms of accuracy, as well as computational cost. Figures 3 and 4 show the results of density of states calculations for a semiconducting (10,0) and metallic (8,8) carbon single wall nanotube (SWNT), respectively. Overall, the accuracy of the ωPBEh results resembles the PBE0 results. In the case of the (10,0) SWNT, the distance between the first two van-Hove singularities (VHS) is 1.0 eV, while the experimental result is 1.1 eV.[34] For the metallic (8,8) nanotube, none of the three methods is in close agreement with experiment (distance between first VHS 1.5 eV[35]). PBE is closest to experiment (2.0 eV), while ωPBEh (2.4 eV) is slightly better than PBE0 (2.7 eV). A detailed comparison of PBE and PBE0 calculations for the density of states of carbon nanotubes will be published elsewhere.[36]

Although the ωPBEh and PBE0 functionals both produce similar results, the computational effort needed to converge these calculations differs significantly. For a metallic (6,6) carbon SWNT (Fig. 1), ωPBEh achieves millihartree accuracy when including the exchange contributions of the first and second nearest neighbors, while interactions up to the fourth nearest neighbors need to be included for PBE0. Including the third nearest neighbors in the ωPBEh calculation results in microhartree accuracy. In the case of PBE0, microhartree accuracy can only be achieved with many more cells and great difficulty, as Fig. 1 shows.

In addition to the faster spatial convergence of the short-range HF interactions, ωPBEh exhibits improved convergence behavior in the self-consistent-field (SCF) procedure. The SR HF exchange interactions can be truncated in a well-behaved manner due to their exponential decay. In several of the metallic systems we have studied, instabilities appear in the SCF procedure when using the standard HF method. The

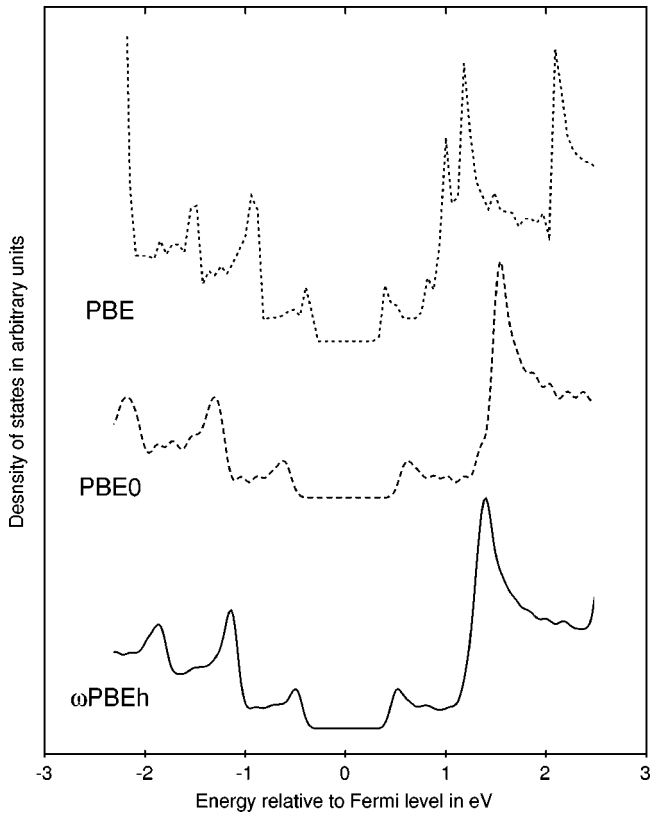

FIG. 3. Density of states for a semiconducting (10,0) carbon single wall nanotube.

TABLE II. ωPBEh/6-311++G(3df,3pd) standard enthalpies of formation at 298 K for the G2 set. All energies and enthalpies in kcal/mol.

Molecule	ΣD_e[a]	ZPE[b]	ΣD_0[c]	$\Delta_f H^\circ_{0\,K}$	$\Delta_f H^\circ_{298\,K}$	$\Delta_f H^\circ_{298\,K}$(Expt.)[d]	Deviation[e]
G2-1 test set							
LiH	54.0	1.8	52.2	37.1	37.1	33.3	3.8
BeH	57.0	2.7	54.3	73.9	74.5	81.7	−7.2
CH	83.2	3.9	79.3	142.3	143.1	142.5	0.6
$CH_2(^3B_1)$	193.7	10.3	183.4	89.9	90.0	93.7	−3.7
$CH_2(^1A_1)$	176.5	10.1	166.4	106.8	106.9	102.8	4.1
CH_3	308.4	17.4	291.1	33.8	33.2	35.0	−1.8
CH_4	417.4	26.8	390.7	−14.2	−16.1	−17.9	1.8
NH	85.6	4.5	81.1	83.1	83.1	85.2	−2.1
NH_2	183.4	11.5	171.8	44.0	43.3	45.1	−1.8
NH_3	294.9	20.7	274.2	−6.7	−8.4	−11.0	2.6
OH	105.9	5.1	100.8	9.8	9.8	9.4	0.4
H_2O	227.1	12.9	214.2	−52.0	−52.7	−57.8	5.1
FH	137.1	5.6	131.6	−61.5	−61.5	−65.1	3.6
$SiH_2(^1A_1)$	147.5	7.1	140.4	69.4	69.0	65.2	3.8
$SiH_2(^3B_1)$	132.3	7.3	125.0	84.9	84.5	86.2	−1.7
SiH_3	223.9	12.8	211.1	50.4	49.1	47.9	1.2
SiH_4	315.9	18.8	297.1	16.0	13.7	8.2	5.5
PH_2	153.8	8.2	145.6	33.1	32.2	33.1	−0.9
PH_3	238.1	14.7	223.5	6.8	4.9	1.3	3.6
H_2S	179.9	9.2	170.7	−1.7	−2.4	−4.9	2.5
HCl	105.2	4.1	101.1	−20.9	−21.0	−22.1	1.1
Li_2	19.6	0.4	19.1	56.3	56.4	51.6	4.8
LiF	134.7	1.3	133.4	−77.2	−77.2	−80.1	2.9
HC≡CH	403.4	16.5	386.9	56.3	56.1	54.2	1.9
CH_2=CH_2	563.2	30.7	532.5	13.9	11.9	12.5	−0.6
CH_3CH_3	711.3	44.7	666.6	−16.9	−20.6	−20.1	−0.5
CN	178.0	2.5	175.5	107.0	107.8	104.9	2.9
HCN	309.9	10.1	299.8	34.3	34.2	31.5	2.7
CO	254.6	3.1	251.5	−22.5	−21.7	−26.4	4.7
CHO	280.3	8.1	272.3	8.3	8.4	10.0	−1.6
CH_2O	372.3	16.4	355.9	−23.7	−24.6	−26.0	1.4
CH_3OH	509.9	31.0	478.9	−43.4	−46.0	−48.0	2.0
N_2	222.2	3.5	218.7	6.4	6.4	0.0	6.4
N_2H_4	437.7	32.5	405.2	26.4	22.9	22.8	0.1
NO	153.3	2.8	150.4	21.1	21.1	21.6	−0.5
O_2	120.8	2.6	118.3	−0.3	−0.3	0.0	−0.3
HOOH	262.2	16.4	245.8	−24.5	−26.0	−32.5	6.5
F_2	32.8	1.6	31.2	5.8	5.7	0.0	5.7
CO_2	391.1	7.1	384.0	−96.0	−96.1	−94.1	−2.0
Na_2	16.1	0.2	15.9	35.4	34.8	34.0	0.8
Si_2	77.0	0.7	76.3	136.9	137.6	139.9	−2.3
P_2	111.1	1.2	110.0	40.9	40.4	34.3	6.1
S_2	105.7	1.0	104.6	26.7	26.7	30.7	−4.0
Cl_2	58.4	0.8	57.6	−0.4	−0.4	0.0	−0.4
NaCl	96.0	0.5	95.6	−41.3	−41.6	−43.6	2.0
SiO	181.9	1.8	180.1	−14.5	−14.3	−24.6	10.3
CS	167.5	1.8	165.6	70.0	70.8	66.9	3.9
SO	124.9	1.7	123.2	1.5	1.4	1.2	0.2
ClO	66.0	1.1	65.0	22.6	22.6	24.2	−1.6
ClF	60.1	1.2	58.9	−11.9	−11.9	−13.2	1.3
Si_2H_6	523.3	29.5	493.7	29.2	25.5	19.1	6.4
CH_3Cl	395.4	22.8	372.6	−19.2	−21.1	−19.6	−1.5
CH_3SH	472.6	27.8	444.8	−2.7	−5.1	−5.5	0.4
HOCl	162.1	8.1	153.9	−14.7	−15.4	−17.8	2.4
SO_2	247.8	4.5	243.3	−59.6	−60.2	−71.0	10.8
G2-2 test set							
Non-hydrogen systems							
BF_3	468.1	7.5	460.6	−269.0	−269.6	−271.4	1.8
BCl_3	331.0	4.5	326.5	−104.5	−104.7	−96.3	−8.4
AlF_3	413.5	4.7	408.8	−275.2	−276.0	−289.0	13.0
$AlCl_3$	307.5	2.8	304.7	−140.7	−141.0	−139.7	−1.3
CF_4	479.7	10.7	468.9	−225.1	−226.4	−223.0	−3.4
CCl_4	319.2	6.1	313.2	−28.8	−29.4	−22.9	−6.5
COS	337.7	5.5	332.2	−37.6	−37.5	−33.1	−4.4
CS_2	283.5	4.1	279.4	21.9	22.1	28.0	−5.9

TABLE II. (*Continued*.)

Molecule	ΣD_e[a]	ZPE[b]	ΣD_0[c]	$\Delta_f H^\circ_{0\,K}$	$\Delta_f H^\circ_{298\,K}$	$\Delta_f H^\circ_{298\,K}$(Expt.)[d]	Deviation[e]
COF_2	422.3	8.8	413.5	−147.6	−148.3	−149.1	0.8
SiF_4	552.4	7.6	544.8	−364.3	−365.5	−386.0	20.5
$SiCl_4$	382.5	4.4	378.1	−157.1	−157.5	−158.4	0.9
N_2O	271.3	6.9	264.4	19.6	18.8	19.6	−0.8
NOCl	191.2	4.0	187.3	12.8	12.4	12.4	0.0
NF_3	208.6	7.1	201.4	−33.5	−34.9	−31.6	−3.3
PF_3	353.8	5.3	348.6	−217.7	−219.0	−229.1	10.1
O_3	133.9	4.9	129.0	48.0	47.3	34.1	13.2
F_2O	88.9	3.8	85.1	10.8	10.2	5.9	4.3
ClF_3	128.0	4.7	123.3	−39.3	−40.3	−38.0	−2.3
$CF_2{=}CF_2$	597.4	13.4	584.0	−170.1	−170.9	−157.4	−13.5
$CCl_2{=}CCl_2$	480.7	9.6	471.0	−16.7	−16.9	−3.0	−13.9
CF_3CN	644.1	14.3	629.8	−121.9	−122.8	−118.4	−4.4
Hydrocarbons							
$CH_3C{\equiv}CH$ (propyne)	706.4	33.7	672.8	43.7	41.9	44.2	−2.3
$CH_2{=}C{=}CH_2$ (allene)	708.5	33.3	675.1	41.3	39.5	45.5	−6.0
C_3H_4 (cyclopropene)	687.5	33.9	653.6	62.9	60.8	66.2	−5.4
$CH_3CH{=}CH_2$ (propylene)	862.2	47.9	814.3	5.4	1.8	4.8	−3.0
C_3H_6 (cyclopropane)	858.2	48.9	809.3	10.4	6.3	12.7	−6.4
C_3H_8 (propane)	1006.7	62.0	944.8	−21.8	−27.1	−25.0	−2.1
C_4H_6 (1,3-butadiene)	1016.8	51.3	965.6	24.1	20.7	26.3	−5.6
C_4H_6 (2-butyne)	1008.2	50.8	957.4	32.3	29.4	34.8	−5.4
C_4H_6 (methylene cyclopropane)	1001.5	51.4	950.1	39.6	35.8	47.9	−12.1
C_4H_6 (bicyclobutane)	996.1	52.2	943.9	45.8	41.7	51.9	−10.2
C_4H_6 (cyclobutene)	1007.5	52.2	955.2	34.5	30.5	37.4	−6.9
C_4H_8 (cyclobutane)	1154.4	66.6	1087.8	5.2	−0.7	6.8	−7.5
C_4H_8 (isobutene)	1161.1	64.8	1096.3	−3.3	−8.4	−4.0	−4.4
C_4H_{10} (butane)	1302.1	79.1	1223.0	−26.8	−33.5	−30.0	−3.5
C_4H_{10} (isobutane)	1302.9	78.9	1224.1	−27.8	−34.7	−32.1	−2.6
C_5H_8 (spiropentane)	1297.3	69.3	1228.0	35.0	29.4	44.3	−14.9
C_6H_6 (benzene)	1383.0	60.3	1322.7	7.0	2.9	19.7	−16.8
Substituted hydrocarbons							
CH_2F_2	437.4	20.2	417.2	−107.0	−108.8	−107.7	−1.1
CHF_3	459.8	15.8	444.1	−167.1	−168.7	−166.6	−2.1
CH_2Cl_2	373.2	18.0	355.3	−24.8	−26.5	−22.8	−3.7
$CHCl_3$	348.4	12.3	336.1	−28.7	−29.9	−24.7	−5.2
CH_3NH_2 (methylamine)	581.0	38.6	542.4	−1.8	−5.4	−5.5	0.1
CH_3CN (methyl cyanide)	616.5	27.4	589.1	18.3	16.6	18.0	−1.4
CH_3NO_2 (nitromethane)	603.9	30.6	573.3	−17.9	−21.0	−17.8	−3.2
CH_3ONO (methyl nitrite)	598.7	30.1	568.6	−13.3	−16.4	−15.9	−0.5
CH_3SiH_3 (methyl silane)	621.2	36.5	584.6	1.7	−2.0	−7.0	5.0
HCOOH (formic acid)	500.5	20.8	479.7	−88.5	−90.3	−90.5	0.2
$HCOOCH_3$ (methyl formate)	786.5	37.9	748.7	−84.2	−87.4	−85.0	−2.4
CH_3CONH_2 (acetamide)	871.5	44.3	827.3	−57.6	−61.3	−57.0	−4.3
C_2H_4NH (aziridine)	724.9	42.6	682.3	28.3	24.4	30.2	−5.8
$(CN)_2$ (cyanogen)	502.6	10.2	492.4	72.6	73.0	73.3	−0.3
$(CH_3)_2NH$ (dimethylamine)	870.5	55.7	814.8	−0.9	−6.1	−4.4	−1.7
$CH_3CH_2NH_2$ (ethylamine)	878.2	55.8	822.5	−8.6	−13.8	−11.3	−2.5
$CH_2{=}C{=}O$ (ketene)	537.4	19.2	518.2	−16.0	−16.8	−11.4	−5.4
C_2H_4O (oxirane)	653.6	34.9	618.7	−13.2	−16.2	−12.6	−3.6
CH_3CHO (acetaldehyde)	677.7	33.6	644.1	−38.7	−41.2	−39.7	−1.5
HCOCHO (glyoxal)	634.8	22.9	611.9	−50.7	−52.1	−50.7	−1.4
CH_3CH_2OH (ethanol)	808.4	48.2	760.2	−51.5	−55.8	−56.2	0.4
CH_3OCH_3 (dimethyl ether)	796.7	48.3	748.4	−39.7	−43.9	−44.0	0.1
C_2H_4S (thiirane)	628.8	33.3	595.5	16.6	13.7	19.6	−5.9
$(CH_3)_2SO$ (dimethyl sulfoxide)	853.0	48.1	804.9	−30.5	−35.0	−36.2	1.2
C_2H_5SH (ethanethiol)	768.5	45.1	723.4	−8.0	−12.0	−11.1	−0.9
CH_3SCH_3 (dimethyl sulfide)	767.5	45.7	721.8	−6.4	−10.4	−8.9	−1.5
$CH_2{=}CHF$ (vinyl fluoride)	575.3	26.7	548.6	−35.3	−37.2	−33.2	−4.0
C_2H_5Cl (ethyl chloride)	693.3	40.1	653.2	−26.5	−29.9	−26.8	−3.1
$CH_2{=}CHCl$ (vinyl chloride)	546.4	25.9	520.5	2.9	1.1	8.9	−7.8
$CH_2{=}CHCN$ (acrylonitrile)	765.4	30.8	734.6	42.8	41.2	43.2	−2.0
CH_3COCH_3 (acetone)	980.6	50.4	930.3	−51.6	−55.4	−51.9	−3.5
CH_3COOH (acetic acid)	803.8	37.5	766.4	−101.9	−105.1	−103.4	−1.7
CH_3COF (acetyl fluoride)	708.5	29.7	678.8	−106.5	−108.8	−105.7	−3.1
CH_3COCl (acetyl chloride)	672.0	28.6	643.4	−61.0	−63.1	−58.0	−5.1

TABLE II. (*Continued.*)

Molecule	ΣD_e[a]	ZPE[b]	ΣD_0[c]	$\Delta_f H^\circ_{0\,K}$	$\Delta_f H^\circ_{298\,K}$	$\Delta_f H^\circ_{298\,K}$(Expt.)[d]	Deviation[e]
$CH_3CH_2CH_2Cl$ (propyl chloride)	988.6	57.2	931.4	−31.5	−36.4	−31.5	−4.9
$(CH_3)_2CHOH$ (isopropanol)	1107.0	65.0	1042.0	−60.0	−65.8	−65.2	−0.6
$C_2H_5OCH_3$ (methyl ethyl ether)	1095.2	65.3	1029.9	−47.9	−53.6	−51.7	−1.9
$(CH_3)_3N$ (trimethylamine)	1161.8	72.6	1089.2	−2.1	−8.9	−5.7	−3.2
C_4H_4O (furan)	1003.8	42.4	961.4	−15.9	−19.1	−8.3	−10.8
C_4H_4S (thiophene)	973.5	40.4	933.1	19.0	16.1	27.5	−11.4
C_4H_5N (pyrrole)	1084.6	49.7	1034.8	15.8	11.8	25.9	−14.1
C_5H_5N (pyridine)	1253.9	53.5	1200.4	20.2	16.2	33.6	−17.4
Inorganic hydrides							
H_2	104.4	5.9	98.5	4.8	4.8	0.0	4.8
SH	86.9	3.7	83.2	34.1	34.1	34.2	−0.1
Radicals							
$C{\equiv}CH$	265.8	8.4	257.4	134.2	135.0	135.1	−0.1
$CH{=}CH_2$ ($^2A'$)	449.3	21.7	427.6	67.2	66.2	71.6	−5.4
CH_3CO ($^2A'$)	585.6	26.1	559.6	−5.7	−7.2	−2.4	−4.8
CH_2OH (^2A)	410.8	22.5	388.3	−4.4	−6.0	−4.1	−1.9
CH_3O ($^2A'$)	403.1	22.6	380.5	3.3	1.5	4.1	−2.6
CH_3CH_2O ($^2A''$)	701.7	39.3	662.5	−5.4	−8.6	−3.7	−4.9
CH_3S ($^2A'$)	384.0	21.6	362.4	28.2	26.4	29.8	−3.4
CH_3CH_2 ($^2A'$)	606.8	35.5	571.3	26.8	24.3	28.9	−4.6
$(CH_3)_2CH$ ($^2A'$)	905.8	53.0	852.8	18.5	14.5	21.5	−7.0
$(CH_3)_3C$ (*t*-butyl radical)	1204.9	70.2	1134.7	9.9	4.5	12.3	−7.8
NO_2	231.4	5.5	225.9	4.6	3.9	7.9	−4.0

[a]Electronic atomization energy.
[b]Zero point energy correction from scaled HF/6-31G* frequency calculation.
[c]Zero point energy corrected atomization energy.
[d]Experimental data compiled in Refs. 32 and 38.
[e]Theory–experiment.

exchange interactions, which need to be truncated in order to make the calculation feasible, are often non-negligible and their truncation leads to instabilities in the SCF. In ωPBEh calculations, only negligible interactions are truncated, resulting in smooth SCF convergence.

TABLE III. Summary of results for enthalpies of formation. All errors in kcal/mol.[a]

	G2-1 set[b]			
Method	MAE[d]	RMS[e]	Max.(−)[f]	Max.(+)[g]
B3LYP	2.46	3.28	−8.2	9.9
PBE	8.19	10.40	−29.1	10.1
PBE0	3.01	3.76	−6.1	10.6
ωPBEh	2.93	3.78	−7.2	10.7
	G2-1andG2-2set[c]			
Method	MAE	RMS	Max.(−)	Max.(+)
B3LYP	3.04	4.40	−8.2	20.0
PBE	17.19	21.00	−50.8	10.1
PBE0	5.15	6.78	−20.8	21.7
ωPBEh	4.16	5.68	−17.4	20.5

[a]6-311++G(3*df*,3*pd*) basis set.
[b]55 molecules.
[c]148 molecules.
[d]Mean absolute error.
[e]Root mean square error.
[f]Maximum negative deviation.
[g]Maximum positive deviation.

V. CONCLUSIONS

We have introduced a new hybrid density functional based on a screened Coulomb operator for the exchange interaction. For molecular systems, this ωPBEh functional yields an accuracy comparable to the best established hybrid methods, such as B3LYP and PBE0. A limited study of PBC calculations also indicates a performance similar to established functionals.

Significant reductions in computational effort can be achieved for large molecules and clusters, especially for systems with relatively small HOMO–LUMO gaps. In these cases, truncation schemes for the HF exchange interaction can benefit greatly from the drastically reduced range of the

TABLE IV. Summary of results for bond length optimization of 25 diatomic molecules[a] in the G2-1 set. All values in Ångstrom.

Method	MAE[b]	RMS[c]	Max.(−)[d]	Max.(+)[e]
B3LYP	0.009	0.013	−0.040	0.028
PBE	0.014	0.017	−0.001	0.054
PBE0	0.009	0.015	−0.038	0.055
ωPBEh	0.008	0.012	−0.035	0.033

[a]Molecules: LiH, BeH, CH, NH, OH, HF, HCl, Li_2, LiF, CN, CO, N_2, NO, O_2, F_2, Na_2, Si_2, P_2, Cl_2, NaCl, SiO, CS, SO, ClO, ClF.
[b]Mean absolute error.
[c]Root mean square error.
[d]Maximum negative deviation.
[e]Maximum positive deviation.

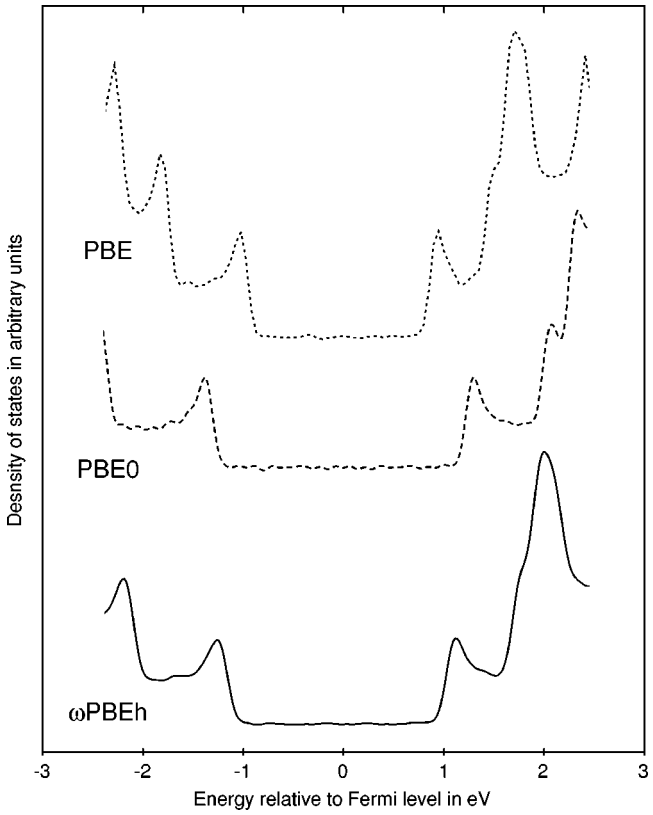

FIG. 4. Density of states for a metallic (8,8) carbon single wall nanotube.

exchange interaction. For PBC calculations in systems with small or no band gaps, the time savings are even larger.

The ωPBEh functional provides an accurate, easy to use, computationally efficient model chemistry which can be applied to a wide range of systems.

ACKNOWLEDGMENTS

This work was supported by the National Science Foundation (Grant No. CHE-9982156) and the Welch Foundation. M.E. acknowledges support through NSERC (Grant No. 238404-01). We would like to thank Viktor Staroverov for his attention to detail in processing the G2 test set data. J.H. also thanks Philippe Ayala and Juanita Jaramillo for countless inspiring discussions.

APPENDIX: INTEGRATING THE ωPBE EXCHANGE HOLE

The original PBE exchange hole[30] is scaled by the Coulomb screening factor $\mathrm{erfc}(\omega y/k_F)$ to yield

$$J^{\omega\mathrm{PBE}}(\rho,s,y)=\left[-\frac{\mathcal{A}}{y^2}\frac{1}{1+(4/9)\mathcal{A}y^2}+\left(\frac{\mathcal{A}}{y^2}+\mathcal{B}+\mathcal{C}[1+s^2\mathcal{F}(s)]y^2+\mathcal{E}[1+s^2\mathcal{G}(s)]y^4\right)\exp(-\mathcal{D}y^2)\right]\times\exp[-s^2\mathcal{H}(s)y^2]\times\mathrm{erfc}\left(\frac{\omega y}{k_\mathrm{F}}\right), \quad \text{(A1)}$$

where $\mathcal{A}$–$\mathcal{H}$ are parameters and parametrized functions of the PBE exchange hole. The integration of this new exchange hole to the enhancement factor could not be carried out analytically for all terms. Specifically, no analytic integral could be found for the following term:

$$\int_0^\infty dy\left[-\frac{\mathcal{A}}{y(1+4/9\mathcal{A}y^2)}+\frac{\mathcal{A}}{y}\exp(-\mathcal{D}y^2)\right]\times\exp[-s^2\mathcal{H}(s)y^2]\mathrm{erfc}\left(\frac{\omega y}{k_\mathrm{F}}\right). \quad \text{(A2)}$$

The problem lies in the terms containing y in the denominator:

$$-\frac{\mathcal{A}}{y(1+4/9\mathcal{A}y^2)}+\frac{\mathcal{A}}{y}\exp(-\mathcal{D}y^2). \quad \text{(A3)}$$

In order to circumvent this obstacle, the term was approximated by a set of five Gaussian-type functions,

$$\mathrm{fit}(y)=ya_1e^{-b_1y^2}+ya_2e^{-b_2y^2}+y^2a_3e^{-b_3y^2}+y^2a_4e^{-b_4y^2}+y^3a_5e^{-b_5y^2}. \quad \text{(A4)}$$

The parameters a_i and b_i were found by nonlinear least squares fit of (A4) to (A3):

$$a_1=-0.000\,205\,484, \quad b_1=0.006\,601\,306,$$
$$a_2=-0.109\,465\,240, \quad b_2=0.259\,931\,140,$$
$$a_3=-0.064\,078\,780, \quad b_3=0.520\,352\,224,$$
$$a_4=-0.008\,181\,735, \quad b_4=0.118\,551\,043,$$
$$a_5=-0.000\,110\,666, \quad b_5=0.046\,003\,777.$$

The quality of the fit was tested by evaluating both the energy contribution and the normalization condition compared to the original expression (A2). The errors were 0.4% and 5%, respectively. Given the use of fitted functions in other terms of the PBE exchange hole, this approximation should not impact the performance of the functional.

Using this approximation, the ωPBE exchange hole (A1) can be integrated to give the enhancement factor as shown in Eq. (9).

[1] J. P. Perdew, Phys. Rev. Lett. **55**, 1665 (1985).
[2] A. D. Becke, J. Chem. Phys. **98**, 5648 (1993).
[3] C. Pisani and R. Dovesi, Int. J. Quantum Chem. **17**, 501 (1980).
[4] K. N. Kudin and G. E. Scuseria, Phys. Rev. B **61**, 16440 (2000).
[5] C. A. White and M. Head-Gordon, Chem. Phys. Lett. **230**, 8 (1994).
[6] J. C. Burant, G. E. Scuseria, and M. J. Frisch, J. Chem. Phys. **105**, 8969 (1996).
[7] G. E. Scuseria, J. Phys. Chem. **103**, 4782 (1999).
[8] L. Greengard and V. Rokhlin, J. Comput. Phys. **73**, 325 (1987).
[9] R. Kutteh, E. Aprà, and J. Nichols, Chem. Phys. Lett. **238**, 173 (1995).
[10] M. C. Strain, G. E. Scuseria, and M. J. Frisch, Science **271**, 51 (1996).
[11] K. N. Kudin and G. E. Scuseria, Chem. Phys. Lett. **289**, 611 (1998).
[12] K. N. Kudin and G. E. Scuseria, Phys. Rev. B **61**, 5141 (2000).
[13] W. Kohn, Int. J. Quantum Chem. **56**, 229 (1995).
[14] E. Schwegler and M. Challacombe, J. Chem. Phys. **105**, 2726 (1996).
[15] C. Ochsenfeld, C. A. White, and M. Head-Gordon, J. Chem. Phys. **109**, 1663 (1998).
[16] D. Pines, *Elementary Excitations in Solids* (Perseus Books, Reading, MA, 1999).
[17] N. W. Ashcroft and N. D. Mermin, *Solid State Physics* (Saunders College Publishing, Orlando, FL, 1976), p. 335.

[18] R. D. Adamson, J. P. Dombroski, and P. M. W. Gill, Chem. Phys. Lett. **254**, 329 (1996).
[19] P. M. W. Gill, R. D. Adamson, and J. A. Pople, Mol. Phys. **88**, 1005 (1996).
[20] A. Savin, *Recent Developments and Applications of Modern Density Functional Theory* (Elsevier, B. V., 1996), pp. 327–357.
[21] H. Iikura, T. Tsuneda, T. Yanai, and H. Hirao, J. Chem. Phys. **115**, 3540 (2001).
[22] J. P. Perdew, M. Ernzerhof, and K. Burke, J. Chem. Phys. **105**, 9982 (1996).
[23] M. Ernzerhof, J. P. Perdew, and K. Burke, Int. J. Quantum Chem. **64**, 285 (1997).
[24] M. Ernzerhof and G. E. Scuseria, J. Chem. Phys. **110**, 5029 (1999).
[25] C. Adamo and V. Barone, J. Chem. Phys. **110**, 6158 (1999).
[26] J. P. Perdew, K. Burke, and M. Ernzerhof, Phys. Rev. Lett. **77**, 3865 (1996).
[27] I. Panas, Chem. Phys. Lett. **245**, 171 (1995).
[28] R. D. Adamson, J. P. Dombroski, and P. M. W. Gill, J. Comput. Chem. **20**, 921 (1999).
[29] P. M. W. Gill and J. A. Pople, Int. J. Quantum Chem. **40**, 753 (1991).
[30] M. Ernzerhof and J. P. Perdew, J. Chem. Phys. **109**, 3313 (1998).
[31] M. J. Frisch, G. W. Trucks, H. B. Schlegel, *et al.*, Gaussian 01, Development Version (Revision B.01+), Gaussian Inc., Pittsburgh, PA, 2001.
[32] L. A. Curtiss, K. Raghavachari, P. C. Redfern, and J. A. Pople, J. Chem. Phys. **106**, 1063 (1997).
[33] K. P. Huber and G. Herzberg, *Molecular Spectra and Molecular Structure* (Van Nostrand Reinhold, New York, 1979).
[34] T. W. Odom, J.-L. Huang, P. Kim, and C. M. Lieber, J. Phys. Chem. B **104**, 2794 (2000).
[35] M. Ouyang, J.-L. Huang, C. L. Cheung, and C. M. Lieber, Science **292**, 702 (2001).
[36] P. V. Avramov, K. N. Kudin, and G. E. Scuseria (unpublished).
[37] S. J. Chakravorty, S. R. Gwaltney, E. R. Davidson, F. A. Parpia, and C. Froese Fischer, Phys. Rev. A **47**, 3649 (1993).
[38] L. A. Curtiss, K. Raghavachari, P. C. Redfern, V. Rassolov, and J. A. Pople, J. Chem. Phys. **109**, 7764 (1998).